DTIC FILE COPY

AD-A224 415

ARL-TR-90-13 Copy No. 16

ACOUSTIC REMOTE SENSING OF PARTICLE MOTION IN THREE DIMENSIONS

FINAL REPORT UNDER CONTRACT N00014-89-J-1231

Nicholas P. Chotiros
Jeff Shorey
Sheila Cheng

APPLIED RESEARCH LABORATORIES
THE UNIVERSITY OF TEXAS AT AUSTIN
POST OFFICE BOX 8029, AUSTIN, TEXAS 78713-8029

DTIC
ELECTE
JUL 25 1990
S D
D

23 May 1990

Final Report

1 November 1988 – 31 October 1989

Approved for public release; distribution is unlimited.

Prepared for:

OFFICE OF THE CHIEF OF NAVAL RESEARCH
DEPARTMENT OF THE NAVY
ARLINGTON, VA 22217-5000

90 07 24 053

UNCLASSIFIED

REPORT DOCUMENTATION PAGE	Form Approved OMB No. 0704-0188

Public reporting burden for this collection of information is estimated to average 1 hour per response, including the time for reviewing instructions, searching existing data sources, gathering and maintaining the data needed, and completing and reviewing the collection of information. Send comments regarding this burden estimate or any other aspect of this collection of information, including suggestions for reducing this burden, to Washington Headquarters Services, Directorate for Information Operations and Reports, 1215 Jefferson Davis Highway, Suite 1204, Arlington, VA 22202-4302, and to the Office of Management and Budget, Paperwork Reduction Project (0704-0188), Washington, DC 20503.

1. AGENCY USE ONLY (Leave blank)	2. REPORT DATE	3. REPORT TYPE AND DATES COVERED
	90-5-23	final 88-11-1 to 89-10-31

4. TITLE AND SUBTITLE
Acoustic Remote Sensing of Particle Motion in Three Dimensions

5. FUNDING NUMBERS
N00014-89-J-1231

6. AUTHOR(S)
Chotiros, Nicholas P. Shorey, Jeff Cheng, Sheila

7. PERFORMING ORGANIZATION NAMES(S) AND ADDRESS(ES)
Applied Research Laboratories
The University of Texas at Austin
P.O. Box 8029
Austin, TX 78713-8029

8. PERFORMING ORGANIZATION REPORT NUMBER
ARL-TR-90-13

9. SPONSORING/MONITORING AGENCY NAME(S) AND ADDRESS(ES)
Office of the Chief of Naval Research
Department of the Navy
Arlington, VA 22217-5000

10. SPONSORING/MONITORING AGENCY REPORT NUMBER

11. SUPPLEMENTARY NOTES

12a. DISTRIBUTION/AVAILABILITY STATEMENT
Approved for public release; distribution is unlimited.

12b. DISTRIBUTION CODE

13. ABSTRACT (Maximum 200 words)
The general objective is to continue development of the remote sensing sonar concept for tracking surface and volume motion of the upper ocean, with or without the aid of detectable scattering layers. A linking algorithm was developed to track the motion of the surface and scattering layers. Optical flow methods were applied to sonar images as an alternative means of tracking volume motion to the coherent remote sensing algorithm reported earlier. The optical flow methods proved to be inappropriate. A number of display formats were explored, and the moving wireframe was found to be most effective. The algorithm and display were extended to the three-dimensional case.

14. SUBJECT TERMS	15. NUMBER OF PAGES
sonar remote sensing correlation flow measurement	41
	16. PRICE CODE

17. SECURITY CLASSIFICATION OF REPORT	18. SECURITY CLASSIFICATION OF THIS PAGE	19. SECURITY CLASSIFICATION OF ABSTRACT	20. LIMITATION OF ABSTRACT
UNCLASSIFIED	UNCLASSIFIED	UNCLASSIFIED	SAR

TABLE OF CONTENTS

DTIC COPY INSPECTED 5

Accession For
NTIS CRA&I
DTIC TAB
Unannounced
Justification
By
Distribution /
Availability Codes
Dist | Avail and / or Special
A-1

LIST OF FIGURES

ACKNOWLEDGMENTS

Several persons made contributions to the work reported here. Jeff Shorey developed the linking algorithm and wrote the corresponding section. Sheila Cheng worked on the optical flow methods. I wish to thank Robert Obrochta, ONR, for his support and for many useful discussions.

1. INTRODUCTION

The ocean surface and scattering layers are strong acoustic targets, and their positions may be estimated and tracked from the range and angle of their acoustic returns. Diffuse volume scatterers may also be tracked but as distributed targets. An algorithm to track volume scatterers has already been described in a previous report.[1] The work reported includes the development of algorithms to address the problem of tracking scattering layers, and the problem of displaying the result in an intuitive and comprehensible manner.

It has been shown by Orr[2] and others that a well-defined scattering layer can be detected by its high backscattering strength. The ocean surface may also be detected in the same way. An algorithm to link signal peaks in adjacent beams was developed for the purpose of estimating the relief of a scattering layer or surface. A sequence of maps generated from a series of pings may then be used to calculate and display the surface motion. A linking algorithm was selected and implemented in software to test its performance in this application. This task complements the development of the volume motion sensing algorithm by providing an independent measure of boundary motion and volume motion in the vicinity of scattering layers.

An alternative method of volume tracking, using optical flow estimation, was attempted. Methods of this type have been demonstrated with some success for optical images. An algorithm was found which could track a discrete target on a sonar display. However, it was unable to adequately track the volume motion of random scatterers, due to the strong scintillation of the acoustic field.

With regard to the problem of volume motion tracking, it became evident very early on that the most pressing problem was the display. The problem of conveying three-dimensional motion information in a comprehensible manner turned out to be formidable. Although more effort was expended on the display than anticipated, at the expense of some of the planned algorithm development tasks, the results obtained were worth the effort. The most comprehensible display was found to be a moving wireframe or grid.

The results of this study will lead to a new type of sonar that can measure three-dimensional motion vectors of the ocean surface and volume. Pointing the sonar towards the ocean surface, the interaction between the surface and the water volume directly beneath the surface may be observed. In conjunction with above-surface instruments, such as optical remote sensing instruments, the interaction between wind, waves, and subsurface currents may be observed. Pointing the sonar into the interior of the ocean, the motion of a variety of ocean phenomena, such as eddy currents, vortices, and internal waves, may be observed, with or without the presence of well defined scattering layers. It should be possible to estimate the curl of the flow field at any point within the field of view, and hence the rate of kinetic energy dissipation.

2. LINKING ALGORITHM

The ocean surface and scatterers suspended in the ocean can be detected by their acoustic backscatter. These data will be meaningful in the sense that the suspended particles will track the movement of the water volume, and therefore can be used as a tool to track wave and volume motion. An algorithm is needed, whereby the movement of the particles can easily be seen in a clean, graphical format. The algorithm, based on line and edge detection methods,[3,4] is designed to be equally applicable to two- and three-dimensional problems. For simplicity, all the following discussion and results will be in a two-dimensional space although the method is equally applicable to three-dimensional problems.

The basic test system consists of two parts: a simulation/analysis portion and a display module. Because of their different functions, FORTRAN and C, respectively, were used to implement them. In doing this, the computation-intensive first section could be done on any computer, preferably a mainframe. The results were then downloaded for display on a Macintosh. For development purposes, an artificial data field was created for test and analysis.

To keep the program realistic, data were simulated in a two-dimensional matrix, all having integer values ranging from 1 to 4096, just as would be received from a 12-bit data collection system. In order for the program to run in a reasonable time, a 100 x 100 resolution cell field was created, consisting of random noise and a half intensity sine wave superimposed. For any given resolution cell (i,j), the unit noise component n_{ij} is given by

$$n_{ij} = \mathrm{rnd}(0,1)^2 \quad , \tag{2.1}$$

where the random number generator rnd(a,b) returns a random number with constant probability density over the open interval (a,b).

The unit signal from a sinusoidal scattering layer s_{ij} is represented by

$$s_{ij} = \begin{cases} 1 \text{ if } \left| j - \left[20 \sin\left(2\pi \frac{i}{50} \right) + 50 \right] \right| \le \frac{1}{2} \\ 0 \text{ otherwise} \end{cases} \quad . \tag{2.2}$$

Therefore, for any given element i,j in the matrix, the total signal e_{ij},

$$e_{ij} = A_n n_{ij} + A_s s_{ij} \quad , \tag{2.3}$$

where A_n is the intensity of the noise and A_s is the intensity of the scattering layer.

Basically, the algorithm must find all the local maxima and link them. The local maxima are selected according to two criteria: peak and absolute level.

$$e_{ij} = \max\{e_{ab}: a=[i-1,i+1], b=[j-1,j+1]\} \tag{2.4}$$

$$e_{ij} \ge e_t \quad , \tag{2.5}$$

where e_t is the absolute threshold. Once all the maxima are found, they are placed in an indexed array for ease of access and processing speed.

Segment selection begins next, where valid pairs of maxima are collected and organized. A segment is simply a line between any two maxima $[i_1,j_1]$ and $[i_2,j_2]$. The points must be nonidentical, and the separation must be within certain bounds. Thus

$$d_l < | [i_1,j_1] - [i_2,j_2] | \le d_u \quad , \tag{2.6}$$

where d_l and d_u are the user defined segment distance limits.

Once the main segment database has been created, there are several filtering techniques which can be applied to it in hopes of regaining the original

flow form. All of the existing research found on the subject were content to use intensity and simple directional filtering.

The first and most fundamental filter is simple thresholding. It was done in the initial segment determination process to limit the size of the data arrays. It would consume an incredible amount of memory to store every possible segment in the whole screen. In fact, it would take n! array entries not counting doubles where n is the number of maxima in the total field. Typically this number ran anywhere from 500 to 1000.

The next way to selectively choose segments is to look at their length, and assign a maximum limit. This limit is the point where the user has determined from the environment that one maximum could really not have anything to do with the other or form anything useful at that distance. This would depend on the density of the scatterers detected in the field.

Another more abstract method of filtering segments is to look at their topology, that is, the relationship of one segment with its connecting segments. There are actually two different methods used with this in mind, the first and simplest being triangular reduction.

With reference to Fig. 2.1(a), the method of triangular reduction is this: given three segments S_1,S_2, S_3 that form a triangle with three and only three unique endpoints, the segment between the two weakest points is eliminated from the list.

A corollary of triangular reduction is vertex reduction. Referring to Fig. 2.1(b), if there exist three segments with four and only four distinct endpoints N_1, N_2, N_3, and N_4, one of which is common to all three segments, then there is a vertex. The main segment field is checked for the recurrence of two of the outer endpoints. The third must not have a connecting segment anywhere in the fie'd and it is eliminated. This results in the removal of little "spines".

The process of checking directional continuity eliminates sharp turns in any of the curves generated in the data field. Referring to Fig. 2.1(c), for any two

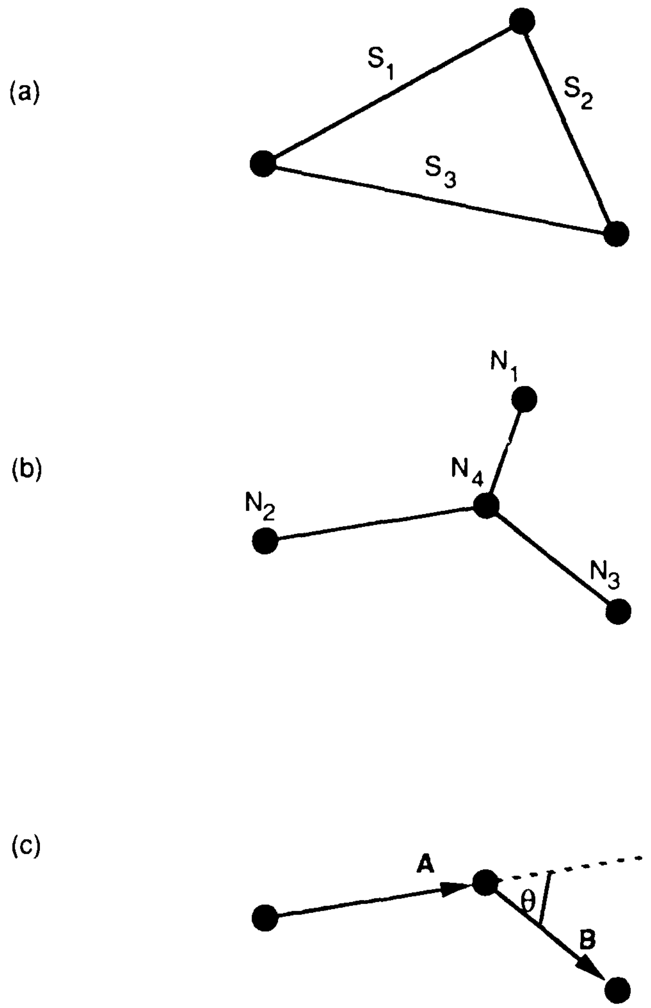

FIGURE 2.1
SEGMENT FILTERING CONSIDERATIONS
(a) TRIANGLE, (b) VERTEX AND (c) DIRECTIONAL CONTINUITY

ARL:UT
AS-90-338
NPC - DS
5 - 29 - 90

vectors **A** and **B** having a common endpoint and separated by an angle θ, it can be stated that

$$\mathbf{A} \cdot \mathbf{B} = |\mathbf{A}|\,|\mathbf{B}| \cos(\theta) \quad . \tag{2.7}$$

The segments are rejected if cos(θ) is less than a predefined threshold.

A final common sense screening method is to eliminate those segments with no endpoints in common with any other segment in the database. This procedure is called Nixstrays after the subroutine name in the program.

Now that the segment database has been filtered to select useful information from amongst the noise, the field is written out into a data file. From there it goes to a separate program, written in C, whose purpose is to plot those data.

There are several user defined parameters in the simulation program. They are the intensity of the sine wave, the minimum threshold for segment qualification, the minimum threshold for maxima qualification, and the maximum segment length, which is the search radius in coordinate units. Some sample plots are included in the following pages along with their parameters.

Figure 2.2 shows a difficult case where the signal-to-background noise ratio is 0 dB; the signal is a sine wave. The result of adding triangular reduction is shown in Fig. 2.3. Parts of sine waves are discernible. The result of further processing by vertex reduction is shown in Fig. 2.4, which shows a reduction in the number of little "spines". Figure 2.5 shows a better situation where the signal-to-background noise ratio is 6 dB. In this case, it was not necessary to use any reduction filter except NixStrays. Clearly, there is no substitute for a moderate signal-to-background ratio.

In conclusion, the decomposition of a data field into segments provides a useful insight into the structure of the data. Various filtering techniques, when applied to these segments, can improve the quality of the display. However, the display is not perfect and still needs careful study by the human eye in order to

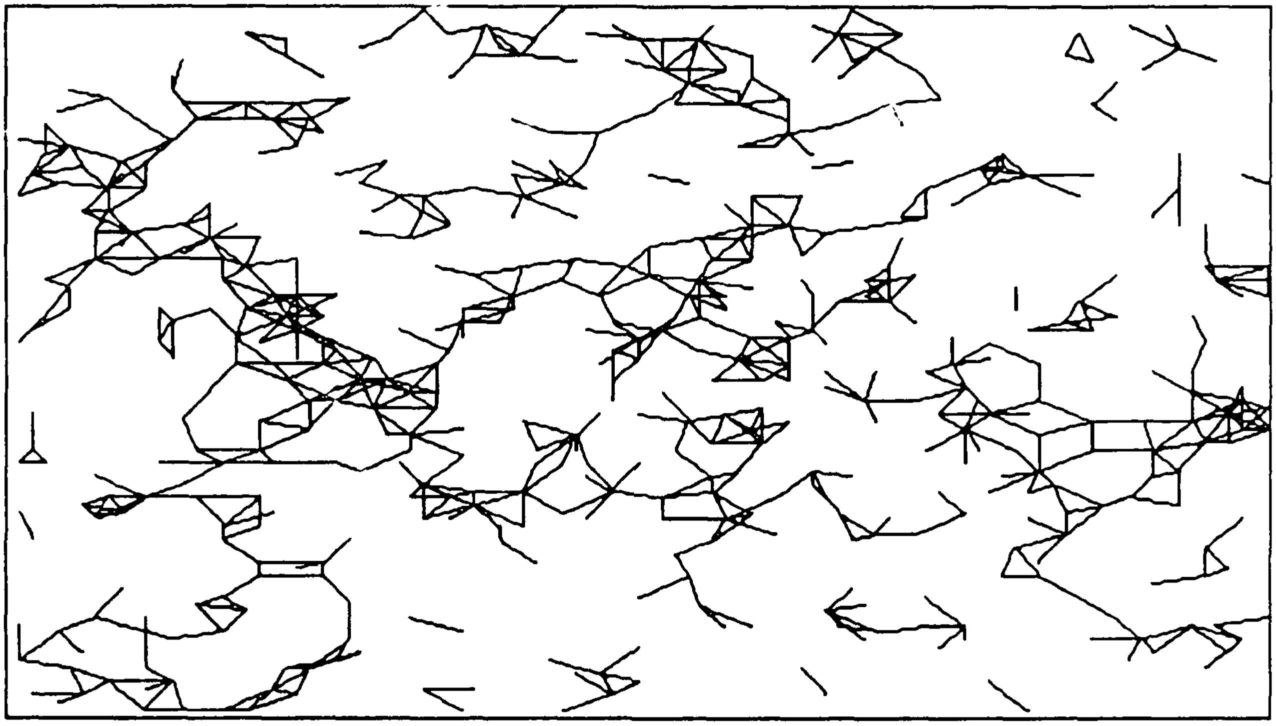

FIGURE 2.2
AN EXAMPLE OF LINKING RESULTS:
A SINUSOIDAL PROFILE EMBEDDED IN NOISE WITH A
SIGNAL-TO-BACKGROUND RATIO OF 0 dB

ARL:UT
AS-90-339
NPC - DS
5 - 29 - 90

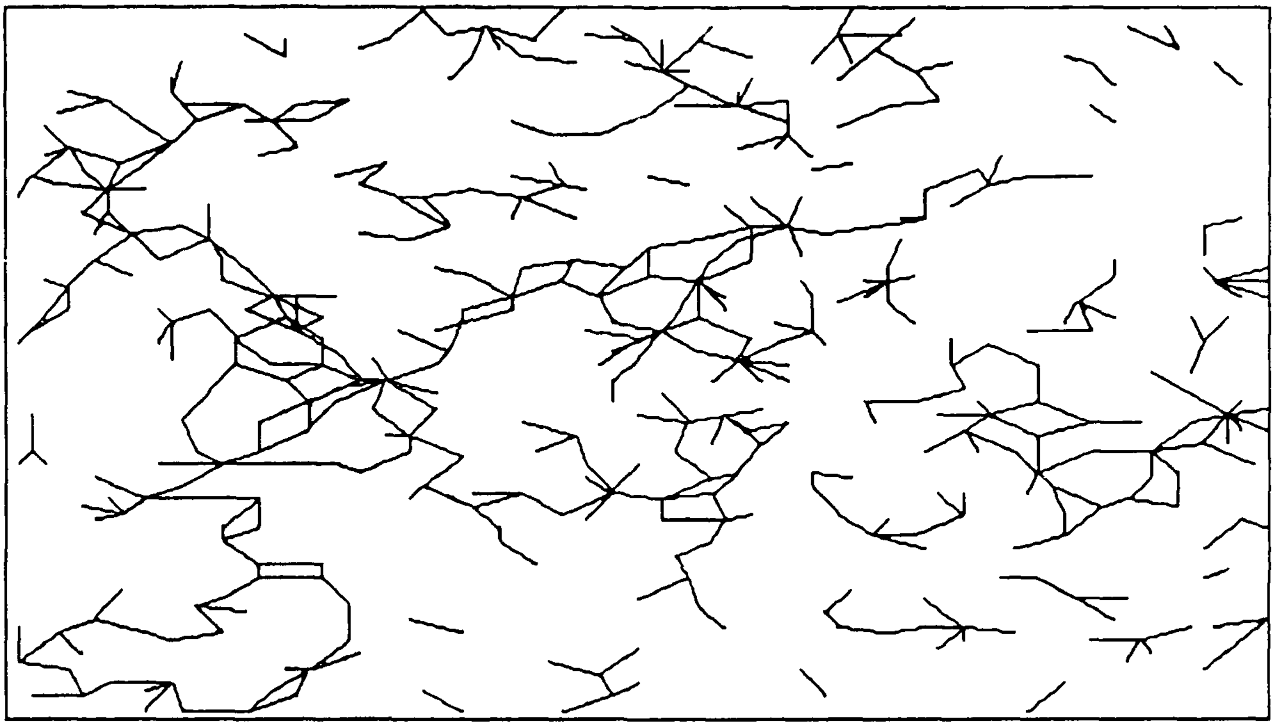

FIGURE 2.3
AN EXAMPLE OF LINKING RESULTS:
A SINUSOIDAL PROFILE EMBEDDED IN NOISE WITH A
SIGNAL-TO-BACKGROUND RATIO OF 0 dB
WITH TRIANGLE REDUCTION

ARL:UT
AS-90-340
NPC - DS
5 - 29 - 90

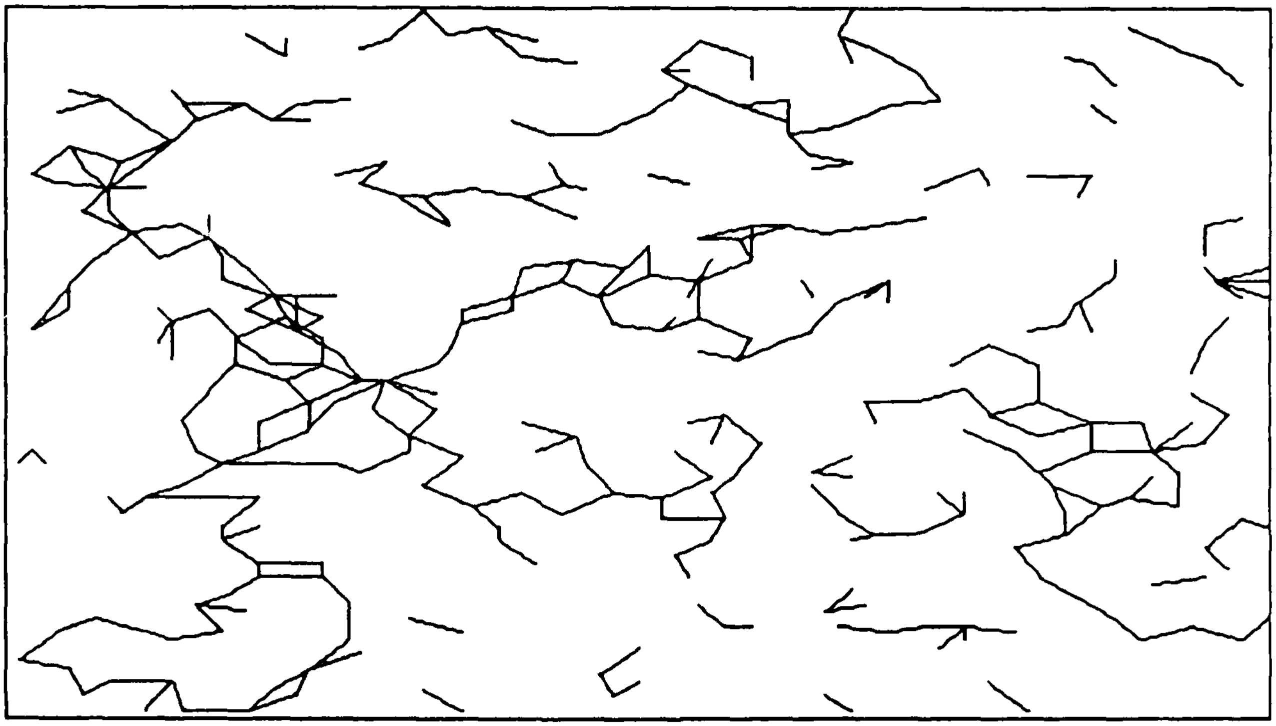

FIGURE 2.4
AN EXAMPLE OF LINKING RESULTS:
A SINUSOIDAL PROFILE EMBEDDED IN NOISE WITH A
SIGNAL-TO-BACKGROUND RATIO OF 0 dB
WITH TRIANGLE AND VERTEX REDUCTION

ARL:UT
AS-90-341
NPC - DS
5 - 29 - 90

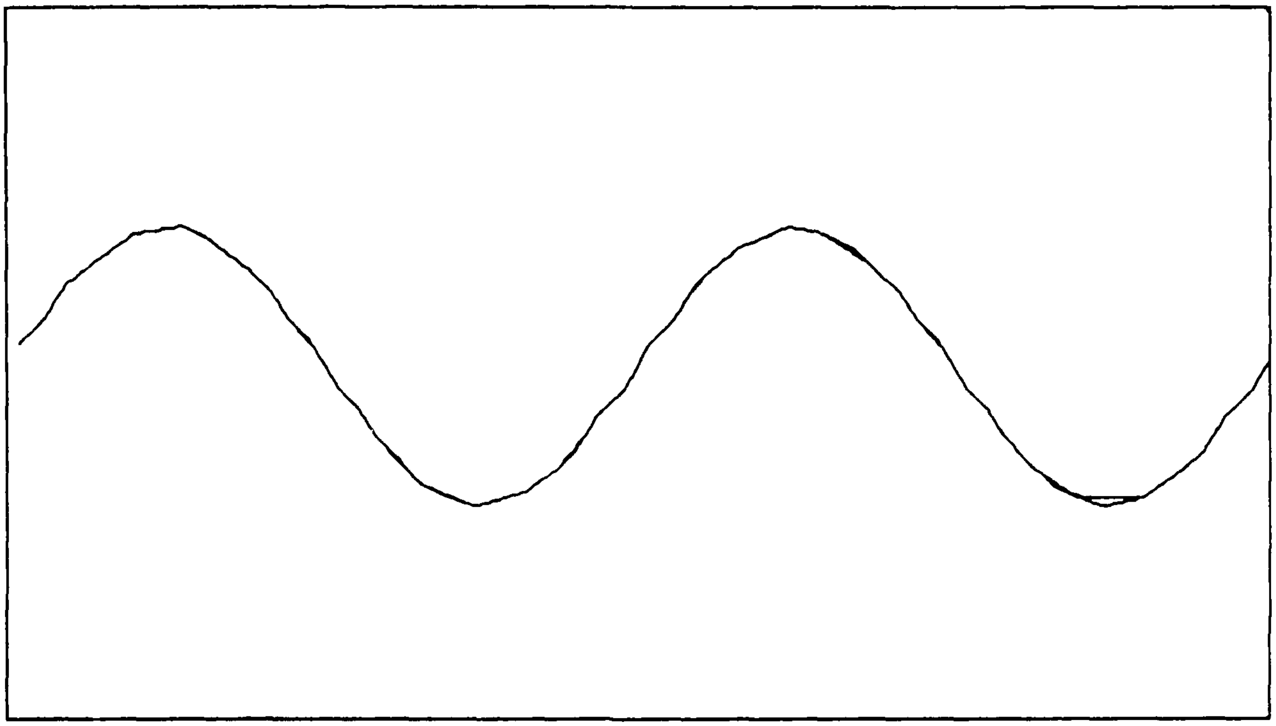

FIGURE 2.5
AN EXAMPLE OF LINKING RESULTS:
A SINUSOIDAL PROFILE EMBEDDED IN NOISE WITH A SIGNAL-TO-BACKGROUND RATIO OF 6 dB

detect a pattern. Perhaps better filters could be developed so as to give a more refined data shape.

The process may be directly applied to the data from a fan of sonar beams. By stacking several fans of beams, one or more surfaces may be mapped out in a three-dimensional space. Thus, the motion of the ocean surface and scattering layers may be observed acoustically.

3. OPTICAL FLOW ESTIMATION

The objective is to track motion from a sequence of sonar images, sampled at a known period, using an optical flow approach. A number of methods based on this approach have been attempted with varying degrees of success. Methods based on edge detection and matching[5,6] are not applicable since sonar images rarely have well defined edges. Methods based on intensity variations, such as those by Yachido et al.[7] and Huang,[8] are most likely to be successful. The method used here is based on that of Huang.

The input data consist of image files in the Image Tool[9] format, which is simply a two-dimensional array of 1 byte pixels. Each pixel is given a color corresponding to its value.

The program reads a series of images and attempts to estimate the optical flow matrix from one image to the next. It involves matching elemental pieces of an image with corresponding areas in subsequent images, and estimating their relative displacement. The underlying assumption is that each image is related to the preceding one by an analytic mapping function, at least piecewise. Consider an image of M by N pixels. Let the image be divided into a matrix of elemental pieces, where each piece is an m by n matrix of pixels. The values of m and n must be chosen such that each piece is small enough that it can be considered as approximately rigid over a sampling period, yet large enough that it contains an adequate number of pixels to make it recognizable from the surrounding pieces.

Assuming a two-dimensional image, let $f_k(i,j)$ and $f_{k+1}(i,j)$ be the intensity, at pixel (i,j), of the k'th and (k+1)'th images, respectively. Referring to Fig. 3.1, consider a piece of the k'th image occupying the rectangle bounded by (i_1,j_1) and (i_1+m, j_1+n). The dissimilarity D between it and a piece in the next image, bounded by $(i_1+\Delta i, j_1+\Delta j)$ and $(i_1+\Delta i+m, j_1+\Delta j+n)$, is defined as

$$D = \sum_{i=i_1}^{i_1+m-1} \sum_{j=j_1}^{j_1+n-1} [f_k(i,j) - f_{k+1}(i+\Delta i, j+\Delta j)]^2 \quad . \tag{3.1}$$

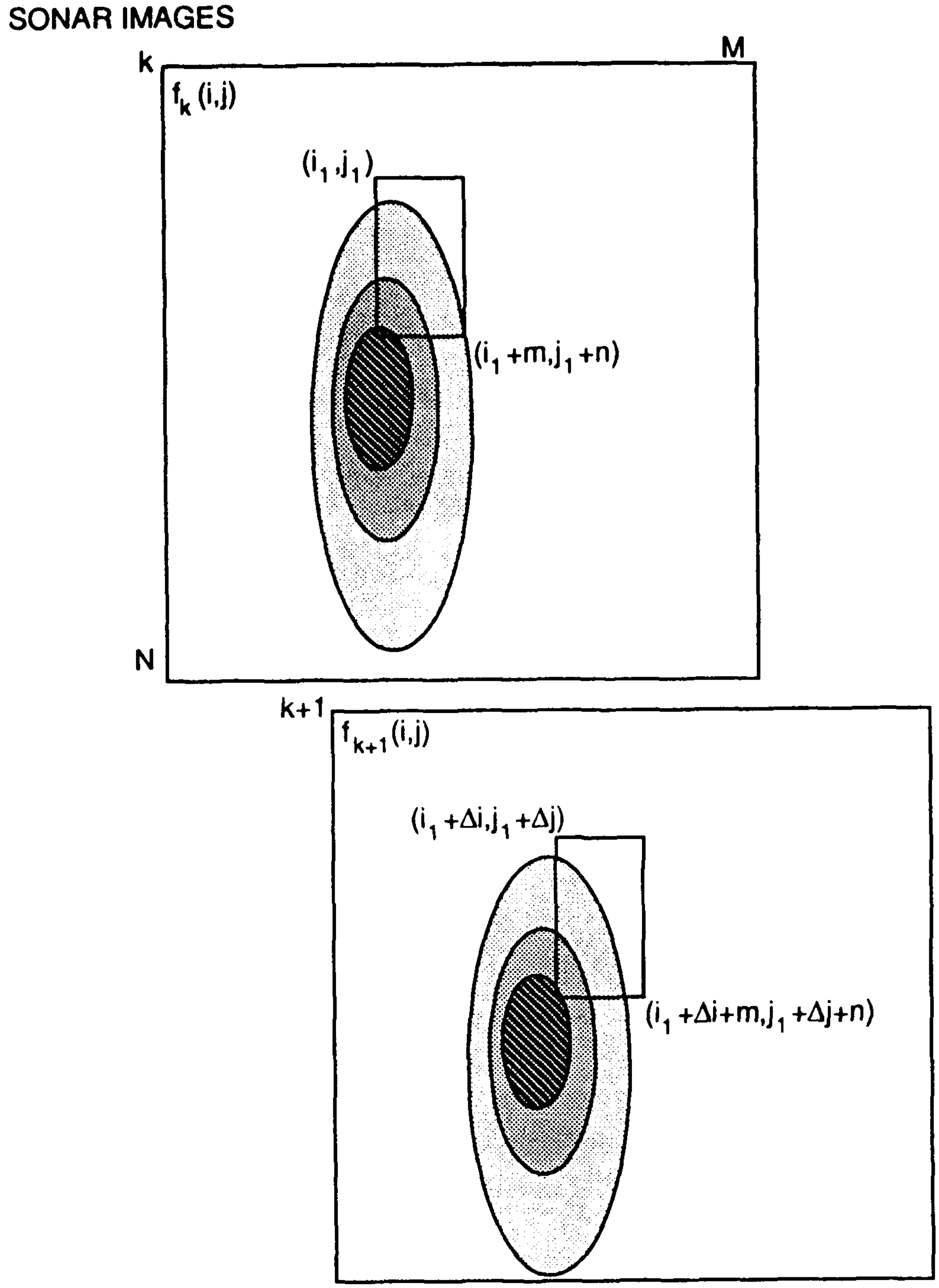

FIGURE 3.1
OPTICAL FLOW CONCEPT

Using a Taylor expansion, Huang obtained a first order approximation of D,

$$D = \sum_{i=i_1}^{i_1+m-1} \sum_{j=j_1}^{j_1+n-1} [\, f_k(i,j) - f_{k+1}(i,j) + \Delta i\, (\partial f_k(i,j)/\partial i) + \Delta j(\partial f_k(i,j)/\partial j)\,]^2 \quad . \qquad (3.2)$$

The minimization of D in Eq. (3.2) is equivalent to the least squares solution for Δi and Δj from the linear set of equations,

$$- f_k(i,j) + f_{k+1}(i,j) = \Delta i\, (\partial f_k(i,j)/\partial i) + \Delta j(\partial f_k(i,j)/\partial j) \quad . \qquad (3.3)$$

The solution assumes that the intensity functions $f_k(i,j)$ and $f_{k+1}(i,j)$ are continuous.

A computer program was written to implement the above first order solution. It was tested on a discrete target, a fluid-filled sphere moving at a constant speed. As an illustration, two frames from a sequence of sonar images of a sphere moving through a fan of beams is shown in Fig. 3.2. It was found that the algorithm could not cope with the fading and scintillation in the sonar images. It was necessary to use the original definition of D and search for the minima by a brute force method.

The algorithm was also tested on distributed scatterers. Three frames from a sequence of images of a moving bubble cloud are shown in Fig. 3.3. It was found that even the brute force method could not track the cloud because of the volatility of its image. As can be seen in Fig. 3.3, the image of the cloud is constantly changing.

Therefore, it was concluded that the optical flow method is not well suited to the tracking of distributed targets such as bubble clouds and scattering layers due to the volatility of the sonar image.

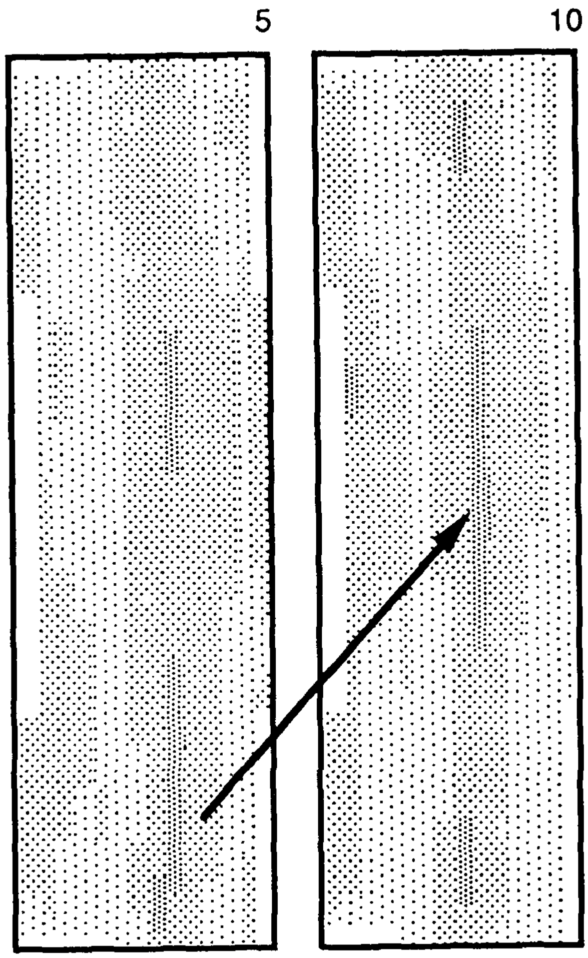

FIGURE 3.2
FRAMES 5 AND 10 FROM A SEQUENCE OF SONAR IMAGES OF A SPHERE MOVING VERTICALLY UPWARDS

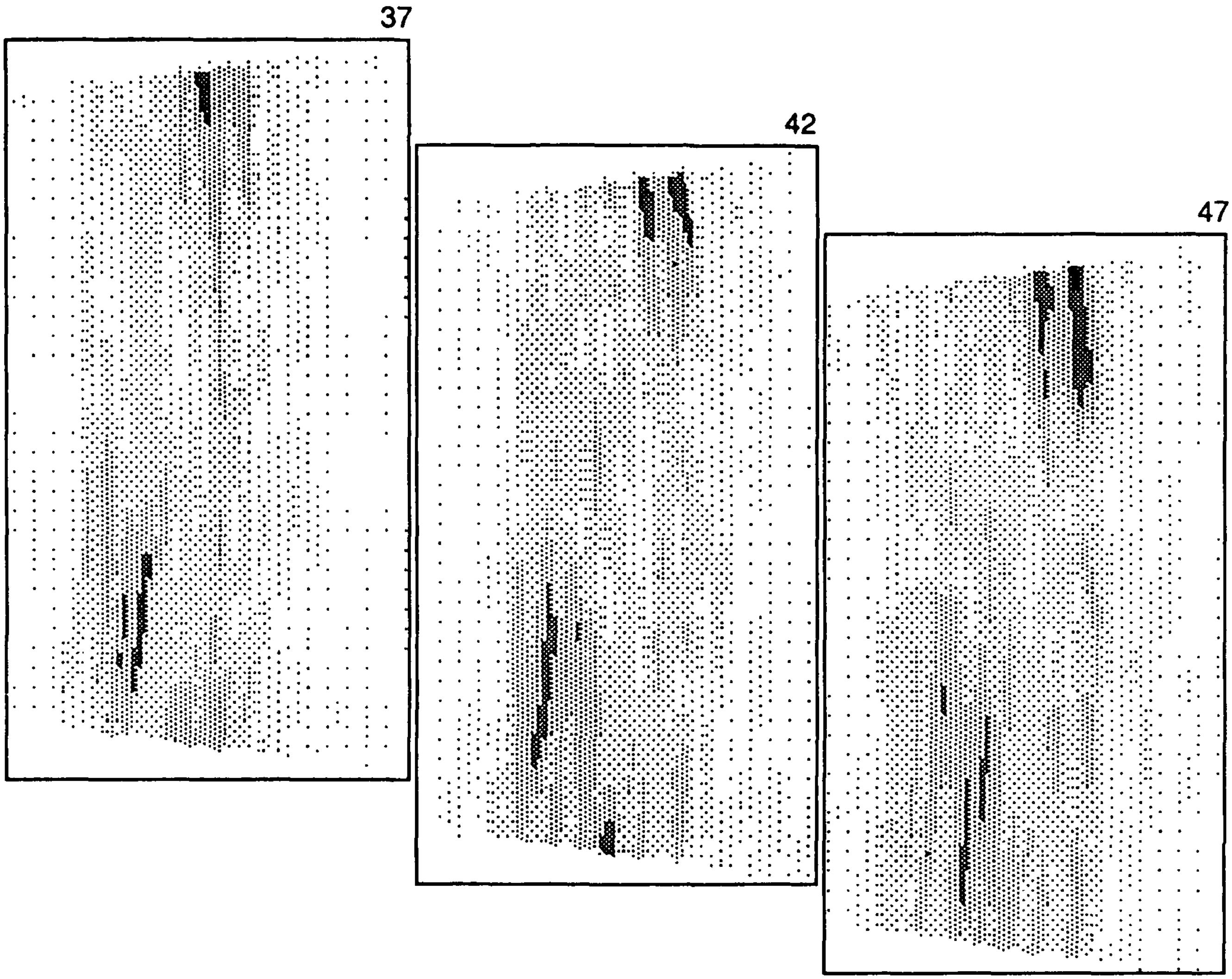

FIGURE 3.3
FRAMES 37, 42, AND 47 FROM A SEQUENCE OF SONAR IMAGES OF A BUBBLE CLOUD RISING FROM THE BOTTOM AND A SCATTERER CLOUD MOVING LEFT TO RIGHT AT THE TOP

4. WIREFRAME DISPLAYS

The two-dimensional irrotational coherent remote sensing (ICRS) algorithm was developed and demonstrated in the preceding reports. Its main problem was the display format. The velocity vector diagrams used in the preceding reports were found to be difficult to comprehend. In this report, they are replaced by wireframe diagrams, which seem to be more intuitive, particularly in moving displays. The wireframes are obtained through the accumulation of the displacement vectors produced by the ICRS algorithm.

The construction of the wireframe images from the displacement vectors computed by ICRS is as follows. The field of view is initially divided into a number of discrete range and bearing cells. Let (i,j) denote the intersection of the i'th beam and j'th range interval. Let $\mathbf{u}(i,j)$ be the displacement vector computed by ICRS. The array of $\mathbf{u}(i,j)$ vectors was interpolated to find the displacement of each node of the wireframe. Consider a node at a vector position $\mathbf{w}_n$ in the n'th ping.

The Cartesian coordinates of $\mathbf{w}_n$ were transformed into polar coordinates (θ_n, r_n). Then, the displacement of the node $\mathbf{v}_n$ was estimated by a simple Gaussian weighting algorithm.

$$\mathbf{v}_n = \frac{\displaystyle\sum_{j=1}^{M}\sum_{j=1}^{N} \mathbf{u}(i,j)\exp\left[-[(\theta_i - \theta_n)/\theta_w]^2 - [(r_i - r_n)/r_w]^2\right]}{\displaystyle\sum_{j=1}^{M}\sum_{j=1}^{N} \exp\left[-[(\theta_i - \theta_n)/\theta_w]^2 - [(r_i - r_n)/r_w]^2\right]}, \tag{4.1}$$

where M and N are the total number of beam and range cells; θ_w and r_w are the beamwidth and range resolution of the system. The position of the node at the (n+1)'th ping is then given by

$$\mathbf{w}_{n+1} = \mathbf{w}_n + \mathbf{v}_n \quad . \tag{4.2}$$

The initial wireframe is an arbitrary reference frame. For maximum efficiency, it should match the resolution cells of the sonar system. However, this is not mandatory. *Other shapes may be preferred* for specific applications. A simple sequence is shown in Fig. 4.1; the reference frame is drawn with broken lines. The actual wireframe is superimposed in solid lines. The sequence of images shows motion in the downrange direction, from simulated acoustic data as processed by the ICRS algorithm. Figures 4.2-4.4 show a representative set of results produced by the algorithm with simulated data.

From previous experimental studies, the results of using the experimental remote sensing sonar to observe the motion of a concrete wall, as illustrated in Fig. 4.5, is shown in Fig. 4.6. The results of observing a stream of hydrogen bubbles, as illustrated in Fig. 4.7, is shown in Fig. 4.8. Finally, the results of looking up into a bubble stream, as illustrated in Fig. 4.9, is shown in Fig. 4.10; in this case the surface was within the field of view, and all points beyond the surface must be surface reflections of scatterers. There appears to be a left-right surface current and out-of-plane currents that the limited line array is unable to properly track, hence the gaps in the display. In all cases, the wireframe format appears to convey an appropriate sense of motion.

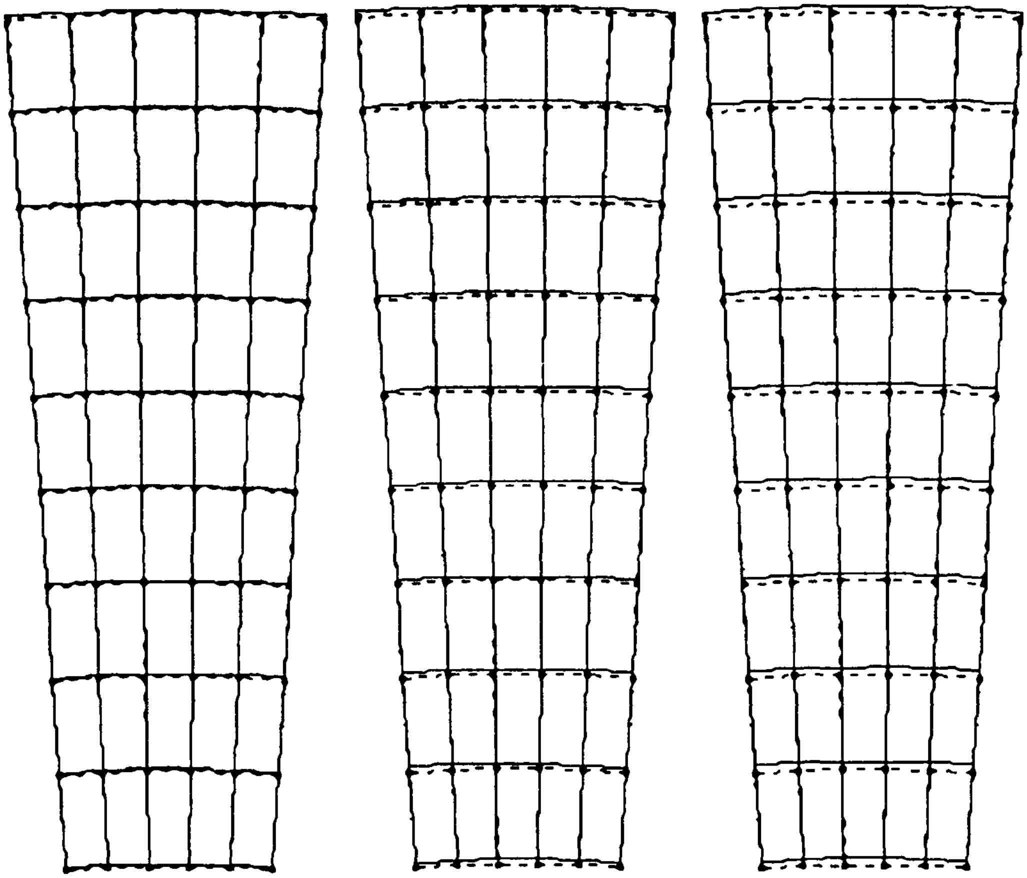

(a) (b) (c)

FIGURE 4.1
SEQUENCE OF THREE WIREFRAME REPRESENTATIONS OF UNIFORM DOWNRANGE MOTION
THE REFERENCE FRAME IS DRAWN WITH BROKEN LINES IN THE BACKGROUND

ARL:UT
AS-90-346
NPC - DS
5 - 29 - 90

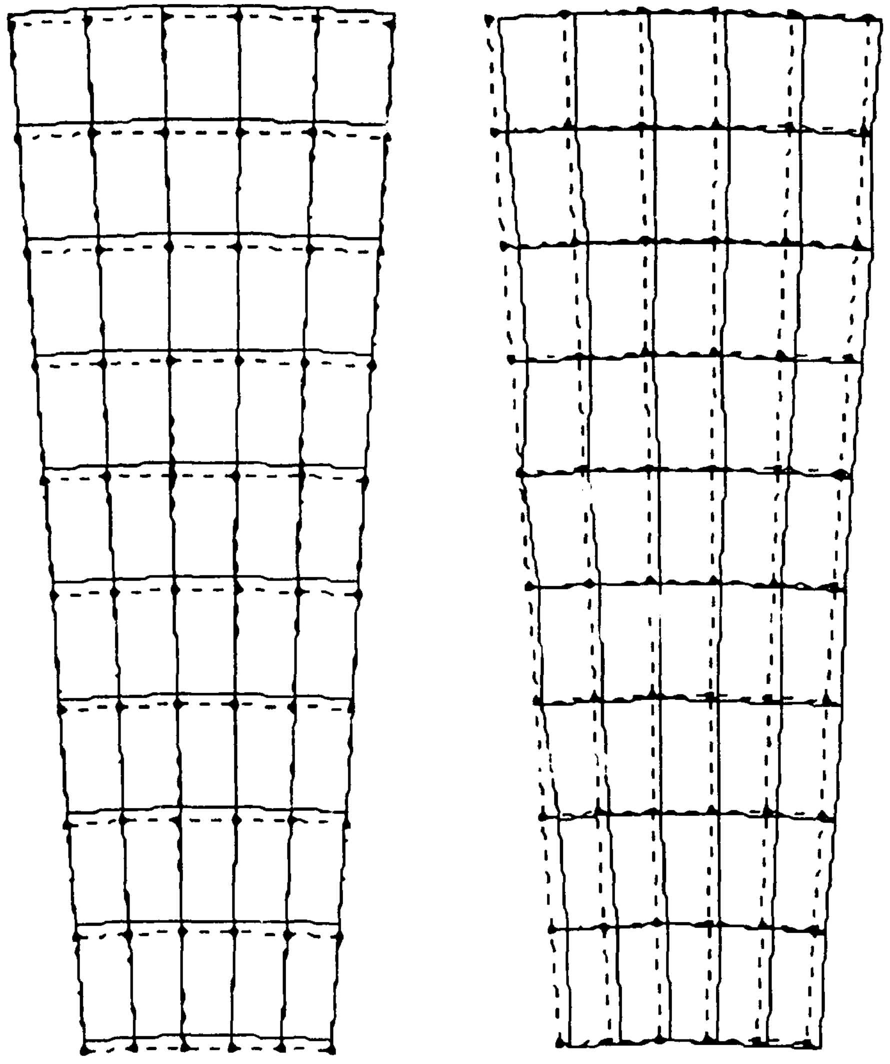

(a) (b)

FIGURE 4.2
COMPARISON OF
(a) DOWNRANGE MOTION AND (b) CROSSRANGE MOTION

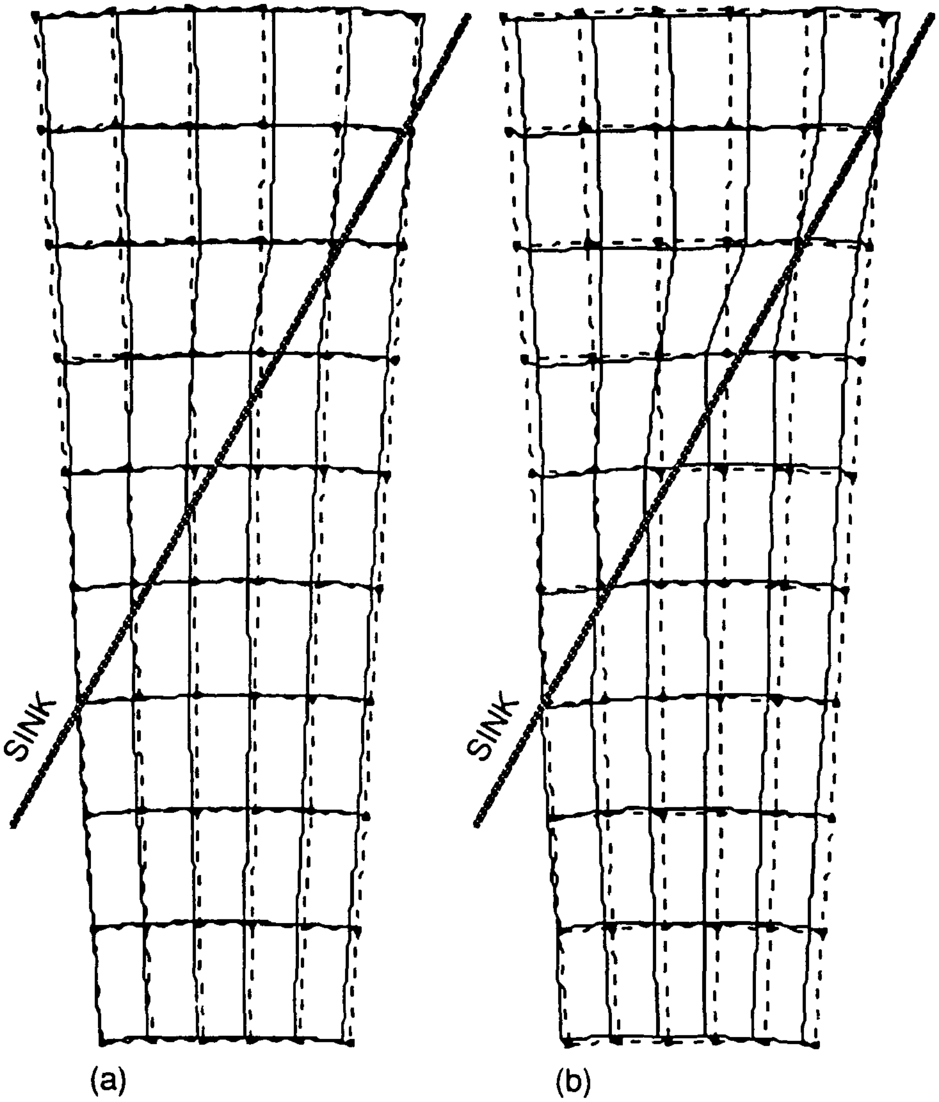

FIGURE 4.3
A SEQUENCE OF WIREFRAMES SHOWING MOTION
TOWARDS A LINE SINK

ARL:UT
AS-90-348
NPC - DS
5 - 29 - 90

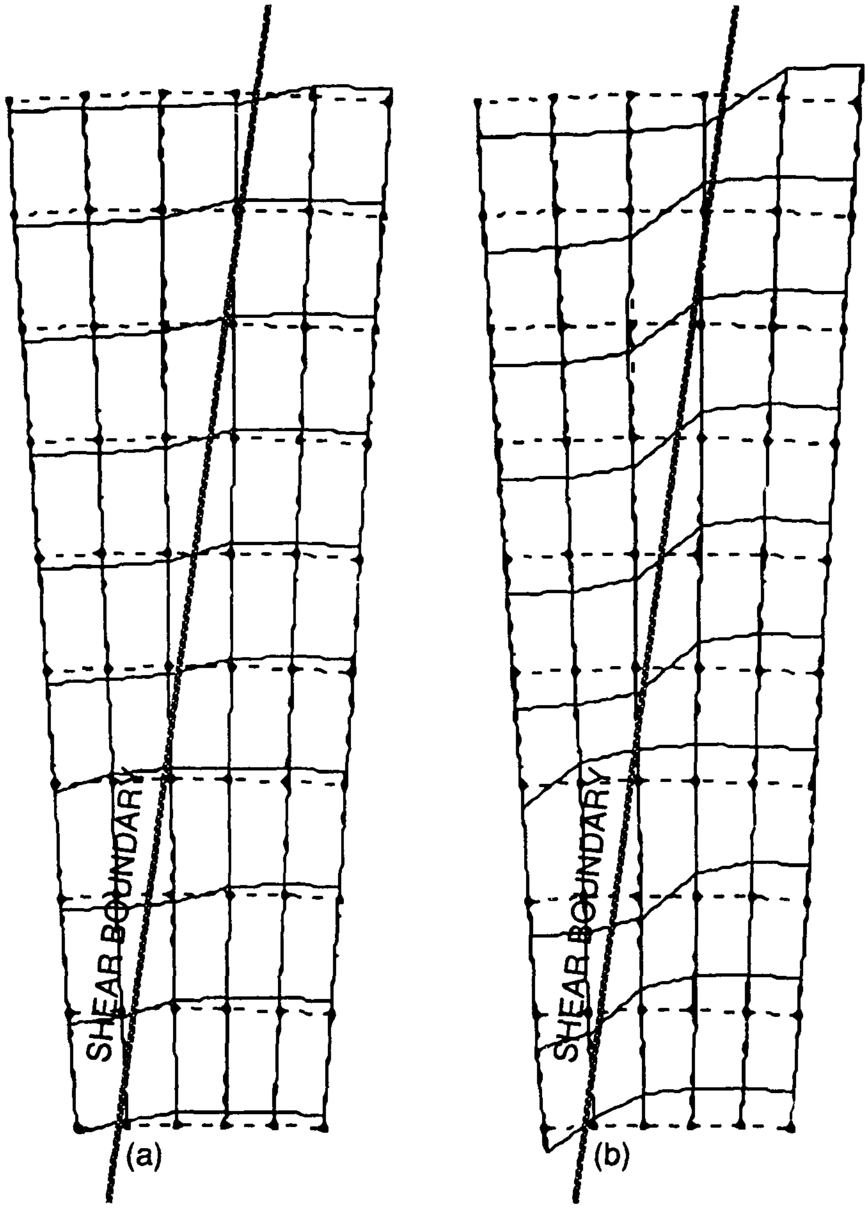

FIGURE 4.4
A SEQUENCE OF WIREFRAMES SHOWING UNIFORM MOTION ABOUT AN ABRUPT SHEAR BOUNDARY

ARL:UT
AS-90-349
NPC - DS
5 - 29 - 90

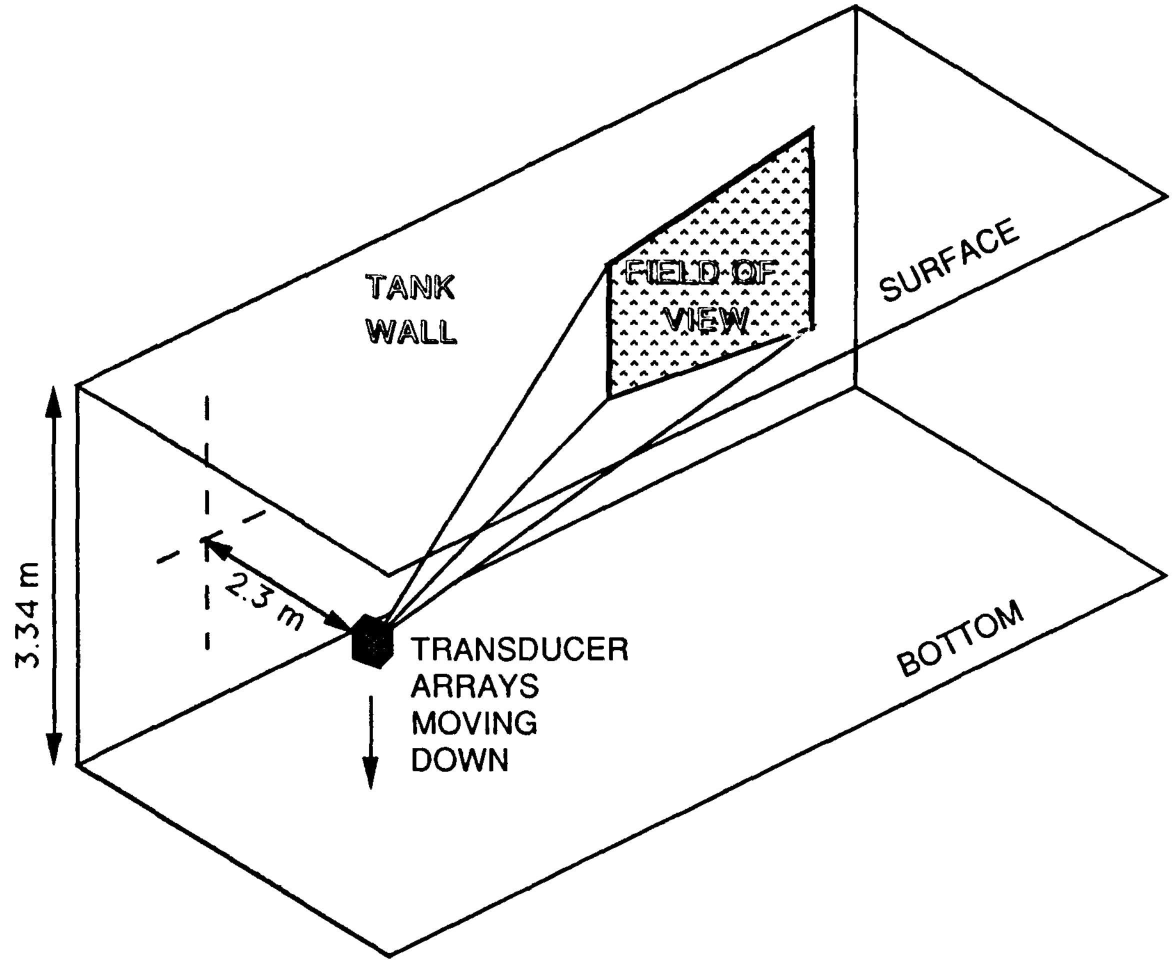

FIGURE 4.5
MOVING WALL EXPERIMENT WITH CONTINUOUS LINE ARRAY

ARL:UT
AS-90-350
NPC - DS
5 - 29 - 90

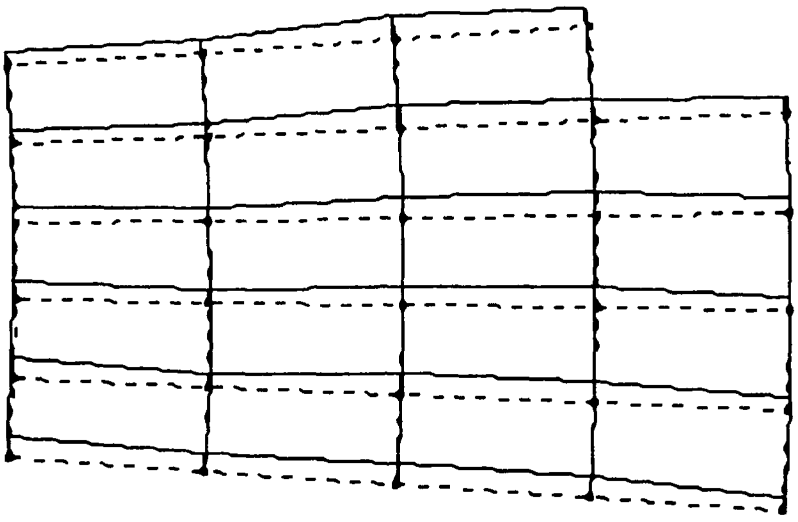

FIGURE 4.6
VERTICAL MOTION OF A CONCRETE WALL
FROM A TANK EXPERIMENT

ARL:UT
AS-90-351
NPC - DS
5 - 29 - 90

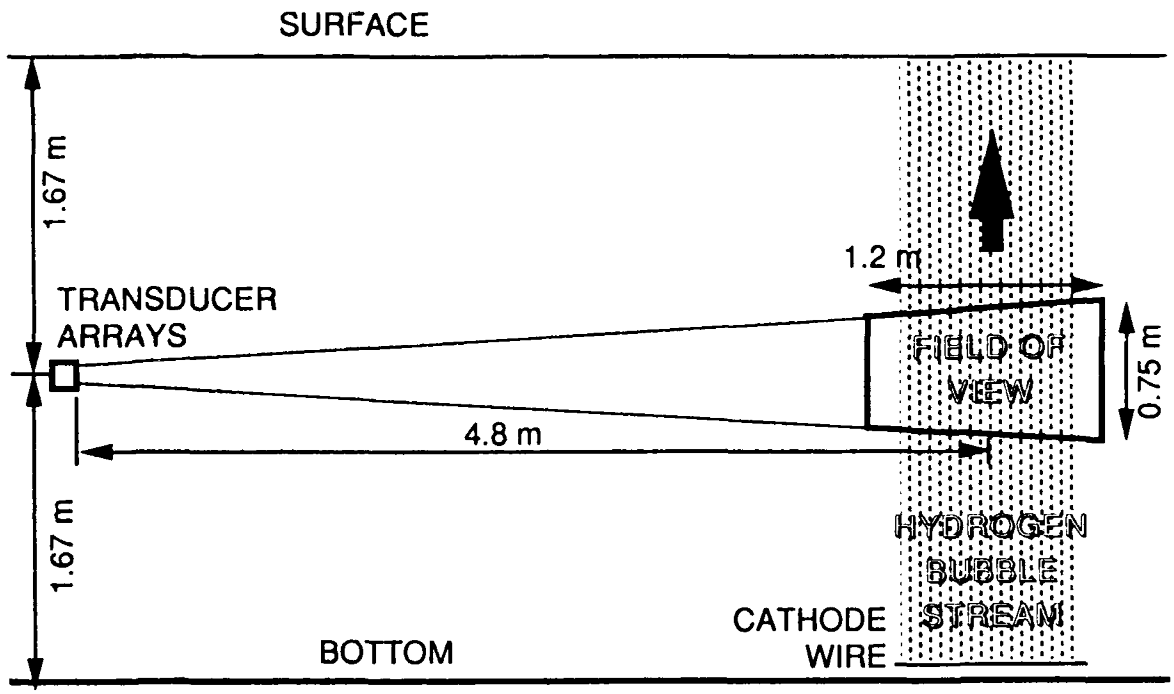

FIGURE 4.7
EXPERIMENT WITH BUBBLE STREAM
IN THE CROSSRANGE DIRECTION

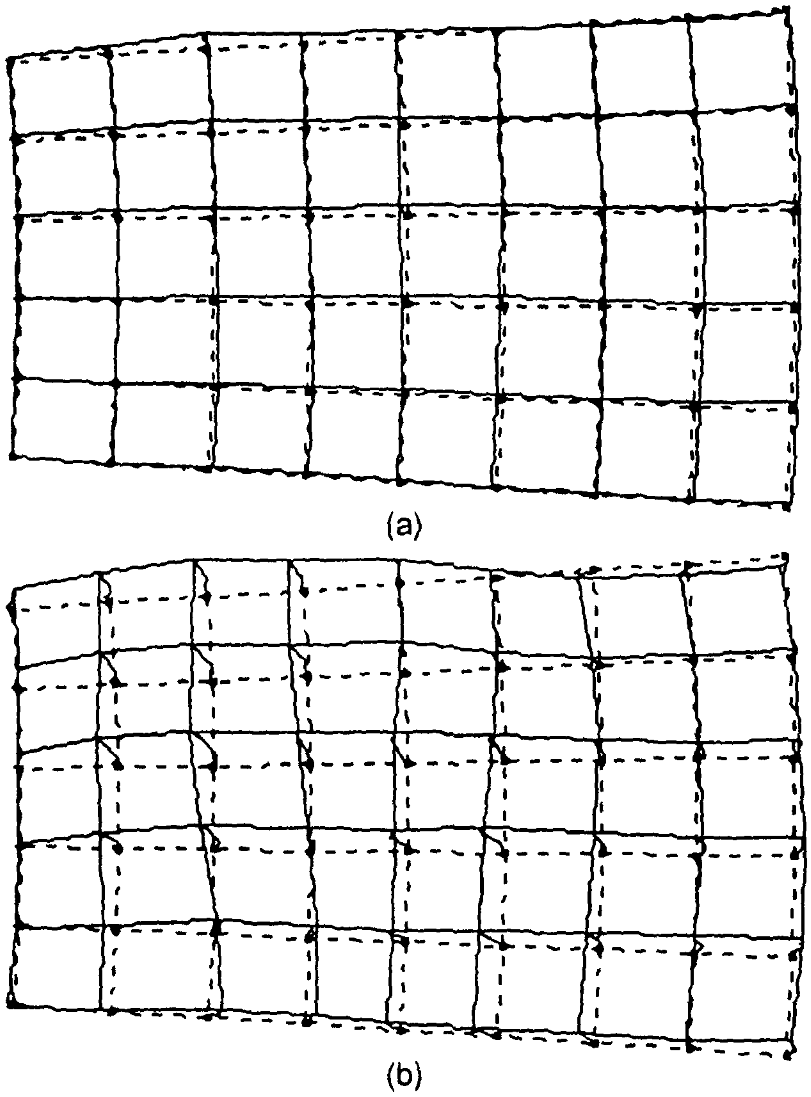

FIGURE 4.8
TWO FRAMES FROM A SEQUENCE OF A HYDROGEN BUBBLE STREAM
OBTAINED IN A TANK EXPERIMENT

ARL:UT
AS-90-353
NPC - DS
5 - 29 - 90

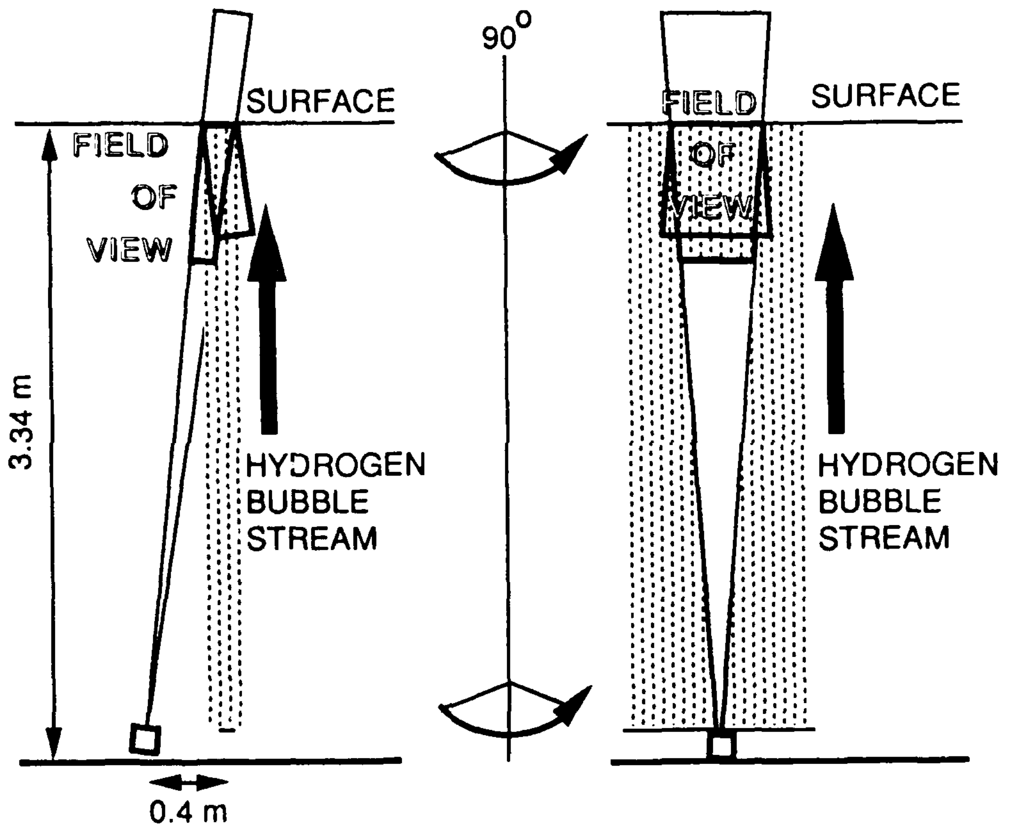

FIGURE 4.9
EXPERIMENT WITH BUBBLE STREAM
IN THE DOWNRANGE DIRECTION

ARL:UT
AS-90-354
NPC - DS
5 - 29 - 90

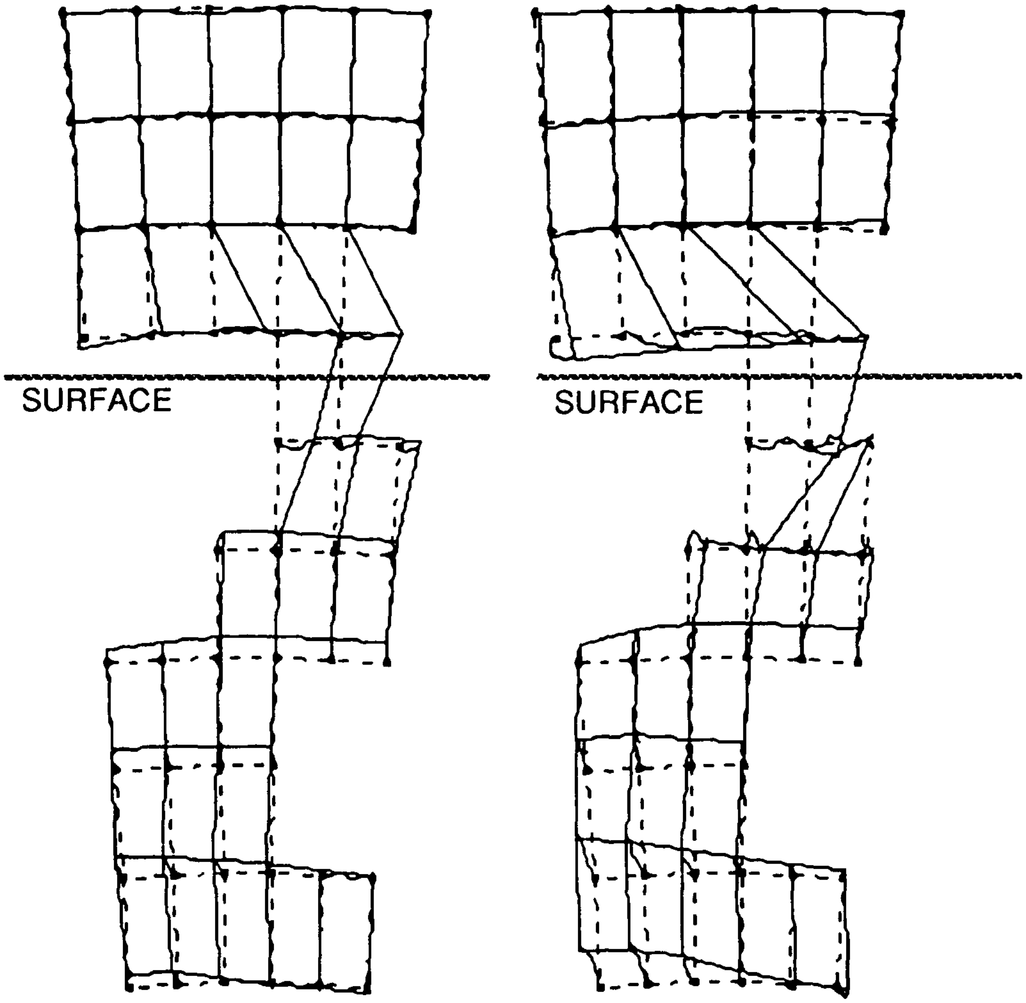

(a) (b)

FIGURE 4.10
TWO FRAMES FROM A SEQUENCE
OF BUBBLE STREAM OBSERVATIONS IN A TANK EXPERIMENT,
INCLUDING THE SURFACE AND SURFACE REFLECTION

ARL:UT
AS-90-355
NPC - DS
5 - 29 - 90

5. THREE-DIMENSIONAL REMOTE SENSING

The two-dimensional irrotational coherent remote sensing (ICRS) algorithm, developed in the preceding reports, can be extended to three-dimensional motion sensing without much difficulty. The difficulty is not expected to be in the motion sensing algorithm, but in the display format. There is an inherent mismatch between three-dimensional motion data and a two-dimensional CRT display. A number of alternatives were considered. The final choice is the wireframe of three adjacent facets. Attempts to show hidden or internal facets were found to be too confusing. The use of color can alleviate the problem but only in certain simple examples.

The construction of the three-dimensional wireframe image is simply an extension of the algorithm used in the two-dimensional case. The field of view is initially divided into a number of discrete range and bearing cells. Let (i,j,k) denote the intersection of the i'th vertical beam, j'th horizontal beam, and k'th range interval. Let **u**(i,j,k) be the displacement vector computed by ICRS. The array of **u**(i,j,k) vectors is interpolated to find the displacement of each node of the wireframe. Consider a node at $\mathbf{w}_n$ in the n'th ping.

The Cartesian coordinates of $\mathbf{w}_n$ were transformed into polar coordinates (θ_n, ϕ_n, r_n). Then the displacement of the node $\mathbf{v}_n$ was estimated by a simple weighting algorithm.

$$\mathbf{v}_n = \frac{\sum_{i=1}^{L}\sum_{j=1}^{M}\sum_{k=1}^{N} \mathbf{u}(i,j,k)\exp\left[-[(\theta_i-\theta_n)/\theta_w]^2 - [(\phi_j-\phi_n)/\phi_w]^2 - [(r_k-r_n)/r_w]^2\right]}{\sum_{i=1}^{L}\sum_{j=1}^{M}\sum_{k=1}^{N} \exp\left[-[(\theta_i-\theta_n)/\theta_w]^2 - [(\phi_j-\phi_n)/\phi_w]^2 - [(r_k-r_n)/r_w]^2\right]}, \qquad (5.1)$$

where L, M, and N are the total numbers of beams and range cells; θ_w, ϕ_w, and r_w are the beamwidths and range resolution of the system. The position of the node at the (n+1)'th ping is then given by

$$\mathbf{w}_{n+1} = \mathbf{w}_n + \mathbf{v}_n \quad . \tag{5.2}$$

To simulate a realistic example of a three-dimensional display that might be obtained by a two-dimensional array, the data from the experimental remote sensing sonar, which contains only a line array, was simply replicated to simulate the missing beam dimension. The resulting displays for the moving bubble cloud experiment of Figs. 4.7 and 4.8 are shown in Fig. 5.1. It is seen that, by limiting the display to only the three outer facets, a perception of three-dimensional motion is conveyed without undue clutter.

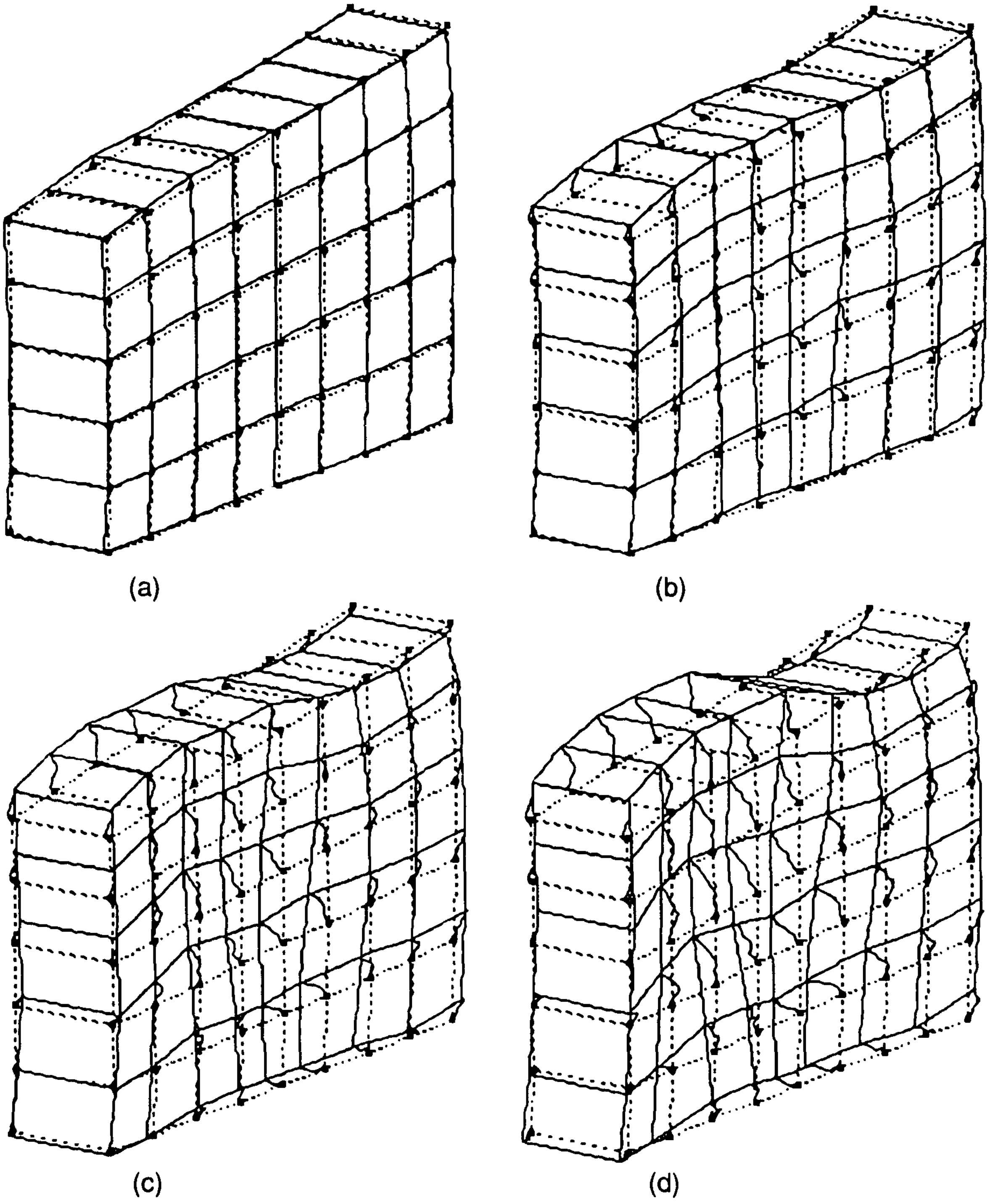

FIGURE 5.1
3-D WIREFRAME OF THREE OUTER FACETS
FOUR FRAMES FROM A SEQUENCE
OBTAINED FROM A HYDROGEN BUBBLE EXPERIMENT

ARL:UT
AS-90-356
NPC - DS
5 - 29 - 90

6. CONCLUSIONS

With respect to the mapping and tracking of the surface and scattering layers, a linking algorithm based on standard clustering methods was developed. It was found to work well in moderate signal-to-background ratio conditions. The method is applicable to both two- and three-dimensional motion.

Motion sensing methods based on optical flow were explored. They employ intensity pattern matching. It was found that the motion of strong discrete targets could be tracked, but not diffuse clouds of scatterers, such as bubble clouds. The difficulty is thought to be the scintillation due to interference effects inherent in any cloud of distributed targets.

With respect to displays, various forms of display were explored. Initially, a moving vector field was used but it proved to be difficult to comprehend. A wireframe format was found to be most effective. A number of examples were used to illustrate its effectiveness.

The two-dimensional ICRS algorithm, developed in the preceding reports, is equally applicable to three-dimensional motion sensing. The main difficulty is perceived to be in the display format. There is an inherent mismatch between three-dimensional motion data and a two-dimensional CRT display. A number of alternatives were considered. Attempts to show hidden or internal facets were found to be too confusing. The use of color can alleviate the problem but only in certain simple examples. The final choice is a wireframe of the nearest three outer facets.

REFERENCES

1. N. P. Chotiros, "Experimental Study of Remote Sensing of Particle Motion by Cross Correlation of Acoustic Backscatter," Final Report under Contract N00014-87-K-0392, Applied Research Laboratories Technical Report No. 89-4 (ARL-TR-89-4), Applied Research Laboratories, The University of Texas at Austin, 7 February 1989.

2. M. H. Orr, "Remote Acoustic Detection of Zooplankton Response to Fluid Processes, Oceanographic Instrumentation and Predators," Can. J. Fish. Aquat. Sci. 38, 1096-1105 (1981).

3. J. B. Burns, A. R. Hanson, and E.M. Riseman, "Extracting Straight Lines," IEEE Trans. Pattern Analysis and Machine Intelligence PAMI-8, No. 4, 425-455 (1986).

4. J. F. Canny, "A Computational Approach to Edge Detection," IEEE Trans. Pattern Analysis and Machine Intelligence PAMI-8, No. 6, 679-698 (1986).

5. J. F. Vesecky et al., "Observation of Sea-Ice Dynamics Using Synthetic Aperture Radar Images: Automated Analysis," IEEE Trans. Geoscience and Remote Sensing 26, No. 1, 38-48 (1988).

6. P. Bouthemy, "A Maximum Likelihood Framework for Determining Moving Edges," IEEE Trans. Pattern Analysis and Machine Intelligence 11, No. 5, 499-511 (1989).

7. M. Yashida, M. Asada, and S. Tsuji, "Automatic Analysis of Moving Images," IEEE Trans. Pattern Analysis and Machine Intelligence PAMI-3, No. 1, 12-20 (1981).

8. T. S. Huang, "Three-Dimensional Motion Analysis by Direct Matching," J. Opt. Soc. Am. 3, No. 9, 1501-1503 (1986).

9. Image Tool v1.2, National Center for Supercomputing Applications, The University of Illinois at Champaign-Urbana, 1989.

23 May 1990

DISTRIBUTION LIST FOR
ARL-TR-90-13
FINAL REPORT UNDER CONTRACT N00014-89-J-1231

Copy No.	
	Office of the Chief of Naval Research Department of the Navy Arlington, VA 22217-5000
1	Attn: R. Obrochta (Code 1125AR)
2	A. Brandt (Code 1122PO)
3	M. Orr (Code 1125AO)
	Director Naval Research Laboratory Washington, DC 20375
4 - 9	Attn: Code 2627
	Director Woods Hole Oceanographic Institution Woods Hole, MA 02543
10	Attn: G. Terray
11	B. Brumley
	The University of Miami Rosensteil School of Marine and Atmospheric Science Division of Morphology and Physical Oceanography Miami, FL 33149
12	Attn: R. Lhermitte
	Director Naval Oceanographic and Atmospheric Research Laboratory Stennis Space Center, MS 39529-5004
13	Attn: R. Farwell (Code 240)
	Commanding Officer Naval Ocean Systems Center San Diego, CA 92152
14	Attn: R. Anderson (Code 54)

Distribution list for ARL-TR-90-13 under Contract N00014-89-J-1231
(cont'd)

Copy No.

	Director
	Department of the Army
	Waterways Experiment Station, Corps of Engineers
	P. O. Box 631
	Vicksburg, MS 39180-0631
15	Attn: T. E. White
16 - 27	Commanding Officer and Director
	Defense Technical Information Center
	Bldg. 5, Cameron Station
	5010 Duke St.
	Alexandria. VA 22314
	Tracor, Inc.
	3420 Kenyon St.
	Suite 209
	San Diego, CA 92110
28	Attn: D. V. Holliday
	Director
	Marine Physical Laboratory
	Scripps Institution of Oceanography
	University of California at San Diego
	La Jolla, CA 92106
29	Attn: R. Pinkel
	The University of Texas at Austin
	Marine Science Center
	Port Aransas, TX 78373-1267
30	Attn: J. Thompson
31	A. Amos
	Science Applications International Corporation
	207 S. Seashore Ave.
	Long Beach, MS 39560
32	Attn: J. K. Lewis
33	Garland R. Barnard, ARL:UT
34	Hollis Boehme, ARL:UT
35	Nicholas P. Chotiros, ARL:UT
36	Harlan G. Frey, ARL:UT

Distribution list for ARL-TR-90-13 under Contract N00014-89-J-1231
(cont'd)

Copy No.	
37	John M. Huckabay, ARL:UT
38	Charles M. Loeffler, ARL:UT
39	Library, ARL:UT
40 - 45	Reserve, ARL:UT